CMS Physics Analysis Summary

Contact: cms-pag-conveners-susy@cern.ch 2012/07/05

Search for supersymmetry in final states with b-jets using the razor variables

The CMS Collaboration

Abstract

A search is performed for squarks and gluinos pairs produced in $\sqrt{s} = 7$ TeV proton-proton collisions with ~ 4.7 fb^{-1} of data collected by the CMS experiment in 2011 at the CERN Large Hadron Collider. The search is sensitive to generic supersymmetry models provided superpartner particles are kinematically accessible and the final state is b-quark enriched, with minimal assumptions on properties of the lightest superpartner particle. The kinematic consistency of the selected events is tested against the hypothesis of heavy particle pair production using the dimensionless *razor* variable R, related to the missing transverse energy E_T^{miss}. The new physics signal is characterized by a broad peak in the distribution of M_R, an event-by-event indicator of the heavy particle mass scale. After background modeling based on data no significant deviation is observed from the Standard Model expectation. The results are interpreted in the context of b-enriched new physics simplified models.

1 Introduction

The third generation plays a special role in many SUSY extensions of the Standard Model (SM). One of the unexplained features of the SM is the hierarchy in the flavor sector, expressed by the big differences in the masses of the quarks (due to the large differences in the Yukawa couplings) and by the hierarchy in the magnitude of the off-diagonal terms of the CKM matrix. It has been proposed that the New Physics (NP) invoked to explain the hierarchy problem of the SM gauge sector could also be the origin of the flavor hierarchy. If this is the case, one would expect the third generation to play a special role in cascade decays of pair-produced SUSY particles at the LHC [1].

Results using the *razor* analysis framework [1] in inclusive final states have been presented by the CMS collaboration using the 2010 and 2011 data [2–4]. Here we present a search for SUSY (and SUSY-like) new physics applying the razor analysis framework to a b-jet enriched dataset. The analysis is designed to kinematically discriminate the pair production of heavy particles from SM backgrounds, without making strong assumptions about the $E_{\mathrm{T}}^{\mathrm{miss}}$ spectrum or details of the decay chains of these particles other than the final state b-jet requirement. The search is largely overlapping with the inclusive search [4], since the kinematic requirements are similar. Requiring a b-tagged jet improves the signal-to-background ratio for SUSY modes with b-jets final states enhancing our discovery potential for such signatures.

The baseline selection requires two or more jets, grouped into two *megajets*. After the requirement of a b-tagged jet the razor analysis tests the consistency, event by event, of the hypothesis that the two megajets represent the visible portion of the decays of two heavy particles.

2 The CMS Apparatus

A description of the CMS detector can be found elsewhere [5]. A characteristic feature of the CMS detector is its superconducting solenoid magnet, of 6 m internal diameter, providing a field of 3.8 T. The silicon pixel and strip tracker, the crystal electromagnetic calorimeter (ECAL) and the brass/scintillator hadron calorimeter (HCAL) are contained within the solenoid. Muons are detected in gas-ionization chambers embedded in the steel return yoke. The ECAL has an energy resolution of better than 0.5 % above 100 GeV. The HCAL combined with the ECAL, measures the jet energy with a resolution $\Delta E/E \approx 100\,\%/\sqrt{E/\,\mathrm{GeV}} \oplus 5\,\%$.

CMS uses a coordinate system with the origin located at the nominal collision point, the x-axis pointing towards the center of the LHC, the y-axis pointing up (perpendicular to the LHC plane), and the z-axis along the counterclockwise beam direction. The azimuthal angle ϕ is measured with respect to the x-axis in the xy plane and the polar angle θ is defined with respect to the z-axis. The pseudorapidity is $\eta = -\ln[\tan(\theta/2)]$.

3 The razor variables

The razor kinematics is based on the generic process of the pair production of two heavy particles, each decaying to an unseen particle plus jets. This includes SUSY signals with complicated and varied decay chains, or the simplest case of a pair of squarks each decaying to a quark and an LSP. All such processes are treated on an equal footing by forcing every event into a dijet topology; this is done by combining all jets in the event into two megajets. When an isolated electron is present, it is included in the megajets if it is clustered as a calorimetric jet with a

[1] We limit our search here to the R-parity conserving SUSY framework.

large-enough transverse momentum. This is not the case for muons, which are invisible to ECAL and HCAL. For the 4.7 fb^{-1} inclusive analysis the trigger requirements, pileup conditions, and pile-up subtraction dictate that isolated electrons enter the megajet reconstruction as jets, while isolated muons are not included in the megajet reconstruction and mimic the contributions of neutrinos. The megajet reconstruction is thus based on a calorimeter-driven view of the events.

We compute the razor analyses grouping a given list of jets in two megajets by defining the two sets of jets with the smallest sum of masses squared.

The four-momenta of the two megajets are used to compute the M_R variable, defined as

$$M_R \equiv \sqrt{(p_{\mathrm{j}_1} + p_{\mathrm{j}_2})^2 - (p_z^{\mathrm{j}_1} + p_z^{\mathrm{j}_2})^2}\,. \tag{1}$$

In Eq. 1 p_{j_i} ($p_z^{\mathrm{j}_2}$) is the absolute value (the longitudinal component) of the ith-megajet momentum.

This variable is computed with the three-momentum of the input megajets. Similarly, one can define the transverse variable:

$$M_T^R \equiv \sqrt{\frac{E_T^{miss}(p_T^{j1} + p_T^{j2}) - \vec{E}_T^{miss}\cdot(\vec{p}_T^{\,j1} + \vec{p}_T^{\,j2})}{2}} \tag{2}$$

from the four-momenta of the two megajets and the missing transverse energy E_T^{miss}. The razor dimensionless ratio is defined as

$$R \equiv \frac{M_T^R}{M_R}\,. \tag{3}$$

4 Monte Carlo Event Samples

The design of the analysis was guided by studies of Monte Carlo event samples generated with the PYTHIA6 [6] and MADGRAPH V4.22 [7] programs, simulated using the CMS GEANT-based [8] detector simulation, and then processed by the same software used to reconstruct real collision data. Events with QCD multijets, top quarks and electroweak bosons where generated with MADGRAPH interfaced with PYTHIA for parton showering, hadronization and the underlying event description. To generate Monte Carlo samples for SUSY the mass spectrum was first calculated with SOFTSUSY [9] and the decays with SUSYHIT [10]. The PYTHIA program was used with the SLHA interface [11] to generate the events. The generator level cross section and the k-factors for the Next-to-Leading Order (NLO) cross section calculation were computed using PROSPINO [12].

5 Event Selection

The analysis uses a set of dedicated triggers, which apply lower thresholds on the values of R and M_R, computed online from the reconstructed jets and E_T^{miss}. Three trigger categories are used: i) hadronic triggers, applying moderate/tight requirements on R and M_R to events with two jets of $p_T > 56$ GeV; ii) muon triggers, similar to the hadronic triggers, but with looser requirements on R and M_R and at least one muon in the central part of the detector with $p_T > 10$ GeV iii) electron triggers, with similar R and M_R requirements and at least one electron of $p_T >$10 GeV, satisfying loose isolation criteria. All of these triggers are fully efficient

in the kinematic regions used for this analysis. In addition, a set of non-razor pre-scaled and unprescaled triggers is used to define the control samples.

Events are required to have at least one good reconstructed interaction vertex [13]. When multiple vertices are found, the one with the highest associated $\sum_{track} p_T^2$ is used. Jets are reconstructed offline from calorimeter energy deposits using the infrared-safe anti-k_T [14] algorithm with radius parameter 0.5. Jets are corrected for the non-uniformity of the calorimeter response in energy and η using Monte Carlo and data derived corrections and are required to have $p_T > 40$ GeV and $|\eta| < 3.0$. The two highest-p_T jets are required to have $p_T > 60$ GeV.

The jet energy scale uncertainty for these corrected jets is 5% [15]. The E_T^{miss} is reconstructed using the particle flow algorithm [16].

The electron and muon reconstruction and identification criteria are described in Ref. [17]. We distinguish tightly-identified electrons and muons (selected requiring the leptons to be isolated in the tracker and in the calorimeters), from loosely-identified electron and muons (having relaxed isolation requirements).

The analysis uses the *medium* working point of the Track-Count High-Efficiency (TCHE) btag algorithm (TCHE output > 3.3) [18]. Only events with at least one b-tagged jet with $p_T > 40$ GeV and $|\eta| < 3.0$ are considered in the analysis.

6 Analysis path

In both simulation and data, the distributions of SM background events with a $b-$tagged jet are seen to have a simple exponential dependence on the razor variables R and M_R over a large fraction of the R^2-M_R plane. The analysis uses simulated events to understand the shapes of the SM background distributions, the number of independent parameters needed to describe them, and extract initial estimates of the values of these parameters. For each of the main SM backgrounds, a control sample is then defined from a subset of the data that is dominated by this particular background in order to obtain a description of the shapes of the background components. A full SM background representation is thus built using statistically independent data samples; this is used as input for a global fit to the remaining data.

The fit is performed in the corner of low M_R and small R^2; the distribution is then extrapolated on an orthogonal region of the R^2-M_R plane, defined such that the two regions overlap when projected on either one of the axes (R^2 or M_R). The fit includes parameters describing the shapes of the R^2-M_R distributions of the SM backgrounds as well as the relative fraction of each background.

The analysis is structured as follows:

- We define a set of exclusive *boxes*, each associated to a given set of HLT paths and a given final state.
- For each box we define a baseline kinematic selection targeting to avoid efficiency trigger turn-on effects. This baseline requirement defines a region in the R^2 vs. M_R plane is which we look for a signal on the 2D kinematic tail.
- We separate the R^2 vs. M_R plane in two regions: i) a *fit region* in the low-R^2/low-M_R corner, where we fit for the shape of the SM background. ii) a *signal region* into which we extrapolate the background model and we characterize a possible signal as an excess on the 2D tail.
- We interpret the results in a limited set of b-enriched simplified models.

We describe each step in the sections that follow.

6.1 Box Definition

We define five exclusive leptonic boxes, filled in a hierarchical order (from the least to the most populated), following the same order adopted in the SUSY inclusive search [4]:

- The MU-ELE box includes the events with at least one muon and one electron.
- The MU-MU box includes the events with at least two muons and no electron.
- The ELE-ELE box includes the events with at least two electrons and no muon.
- The MU box includes the events with one muon and no electron.
- The ELE box includes the events with one electron and no muon.
- A HAD box, with all the selected events which don't enter any of the other boxes.

Once the razor variables are computed, a box-dependent baseline selection is applied:

- $M_R > 300$ GeV and $0.11 < R^2 < 0.50$ for the leptonic boxes.
- $M_R > 400$ GeV and $0.18 < R^2 < 0.50$ for the HAD box.

The selection is driven by the need of a flat trigger efficiency.

6.2 Fit Region and Signal Regions

In each box we define six signal regions, shown by the S_i rectangles in Fig. 3 and Fig. 4. We use a common definition of the signal regions, uniform across the boxes and consistent with the inclusive razor analysis. These regions are used to establish the level of agreement between the data observed and the expected background.

The green delineated regions represent the fit regions, used to determine the background model which is the extrapolated to the signal-sensitive large-M_R/largeR^2 region. The boundaries of the fit regions give the minimal choice for a stable fit with the available luminosity.

7 The Background Model

We perform an extended and unbinned maximum likelihood (ML) fit, using the ROOFIT fitting tool [19]. For each box, the fit is performed in the portion of the R^2-M_R plane delimited by the green shaded regions. We refer to this region as the *fit region*. The fit provides a full description of the SM background in the R^2-M_R plane in each box. The likelihood function for a given box is written as [20]:

$$\mathcal{L} = \frac{e^{-(\sum_{SM} N_{SM})}}{N!} \prod_{i=1}^{N} (\sum_{SM} N_{SM} P_{SM}(M_R, R^2)) \tag{4}$$

where N_{SM} is the number of events for each SM background and the associated pdf $P_{SM}(M_R, R^2)$ is written as

$$P_{SM}(M_R, R^2) = (1 - f_2^{SM}) \times F_{SM}^{1st}(M_R, R^2) + f_2^{SM} \times F_{SM}^{2nd}(M_R, R^2) \tag{5}$$

with

$$F(M_R, R^2) = \left[b(M_R - M_R^0)(R^2 - R_0^2) - 1\right] e^{-b(M_R - M_R^0)(R^2 - R_0^2)}. \tag{6}$$

We note that the determination of the second component in the single-lepton boxes is used as input in the other fits.

Once this parameterization is determined, it is used to estimate the total SM background yield in regions where a SUSY or other new physics signal would be visible. In the absence of such a signal, the background shape is used to constrain the parameters of the new physics model under consideration.

We perform the fit to the background shapes in the regions delineated by the green shaded regions in Fig. 3 and Fig. 4. The result of the ML fit projected on M_R and R^2 is shown in Fig. 1 for the dilepton boxes and Fig 2 for the MU, ELE and HAD boxes.

Using the background model returned by the ML fit, we derive the distribution of the expected yield in each SR using pseudo-experiments.

In order to correctly account for correlations and uncertainties on the parameters describing the background model, the shape parameters used to generate each pseudo-experiment dataset are sampled from the covariance matrix returned by the ML fit. The actual number of events in each dataset is then drawn from a Poisson distribution centered on the yield returned by the covariance-matrix sampling. For each pseudo-experiment dataset, the number of events in the SR is found. For each of the SR, the distribution of the number of events derived by the pseudo-experiments is used to calculate a two-sided p-value, corresponding to the probability of observing an equal or less probable outcome for a counting experiment in each SR. The p-values obtained are quoted in Fig. 3 and Fig. 4. In the same figures, we quote the median and the mode of the yield distribution for each SR, together with the observed yield. A 68% probability interval is also calculated, using the probability associated to each yield outcome as the ordering principle.

No significant deviation is observed, which indicates the compatibility of the background model to the data and the absence of a significant excess from non-SM processes.

8 Interpretation of the Results

We interpret the result of the fit+extrapolation procedure in terms of an exclusion limit on simplified models. In simplified models, introduced in Refs. [21, 22], a limited set of hypothetical particles and decay chains are introduced to produce a given topological signature. Specific applications of these ideas have appeared in Refs. [23–25]. We consider two models i) sbottom pair production, with each sbottom squark decaying to a b quark and a neutralino; ii) gluino pair production, with each gluino decaying in a $b\bar{b}$ pair and a neutralino.

We set a 95% confidence-level (CL) limit across the plane identified by the mass of the mother particle (gluino or sbottom) and the LSP mass, using the *hybrid* CLs procedure. We take as input:

- the likelihood at the minimum for the background, as returned by the ML fit in the fit region for each box,
- the 2D distribution in the R^2 vs M_R plane for the considered signal model,
- a cross section for the considered signal, which allows us to set a normalization.

The limit procedure is applied as a function of the signal cross section. Two likelihood functions are defined: The signal plus background likelihood and the background-only likelihood. The

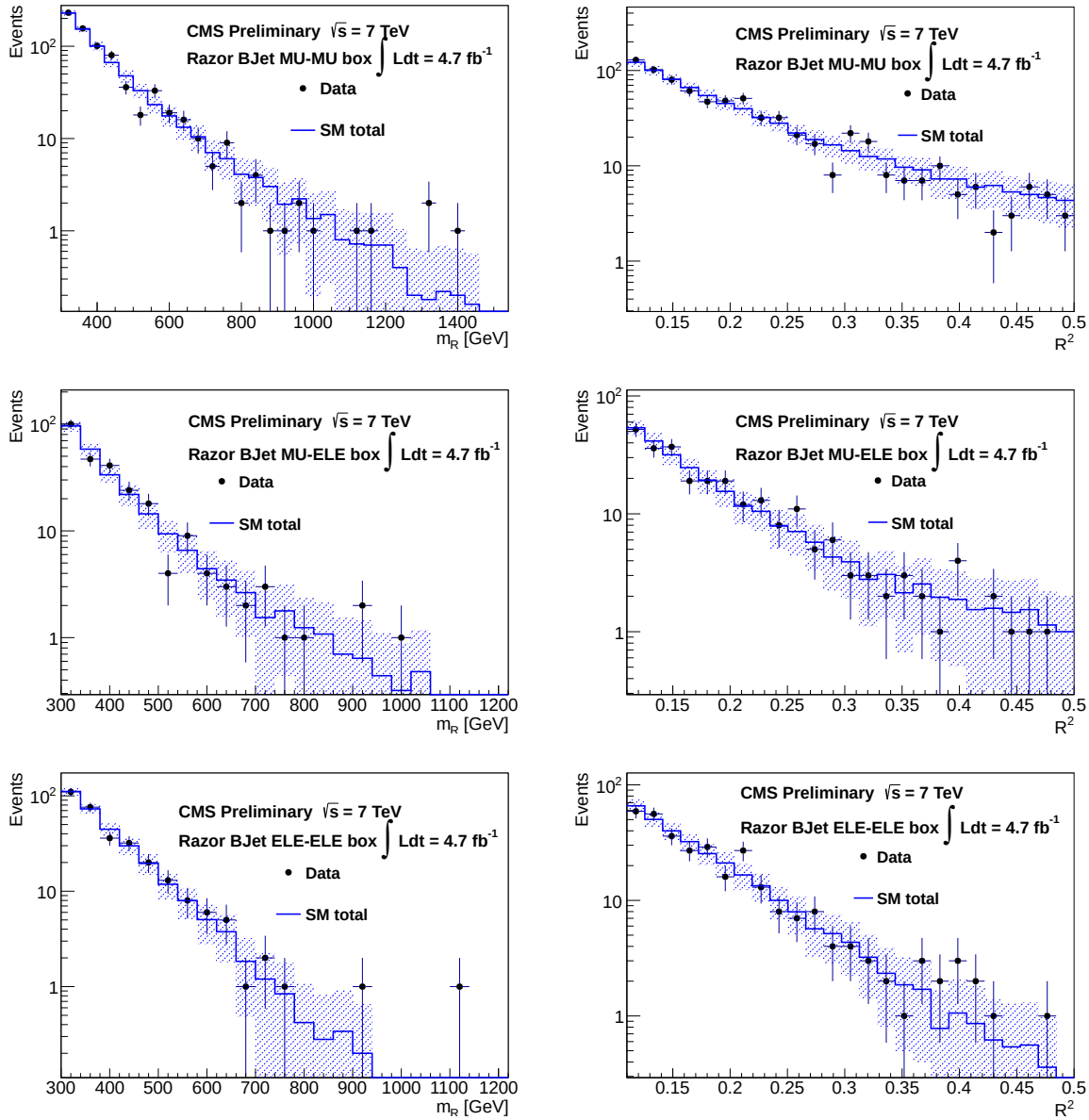

Figure 1: Projection of the 2D fit result on M_R (left) and R^2 (right) for the MU-MU, MU-ELE and ELE-ELE b-tagged boxes using the razor datasets.The blue histogram is the total Standard Model prediction as obtained from a single pseudo-experiment based on the 2D fit. The fit is performed in the R^2-M_R sideband and projected into the full region. Only the statistical error on the total SM background prediction is shown.

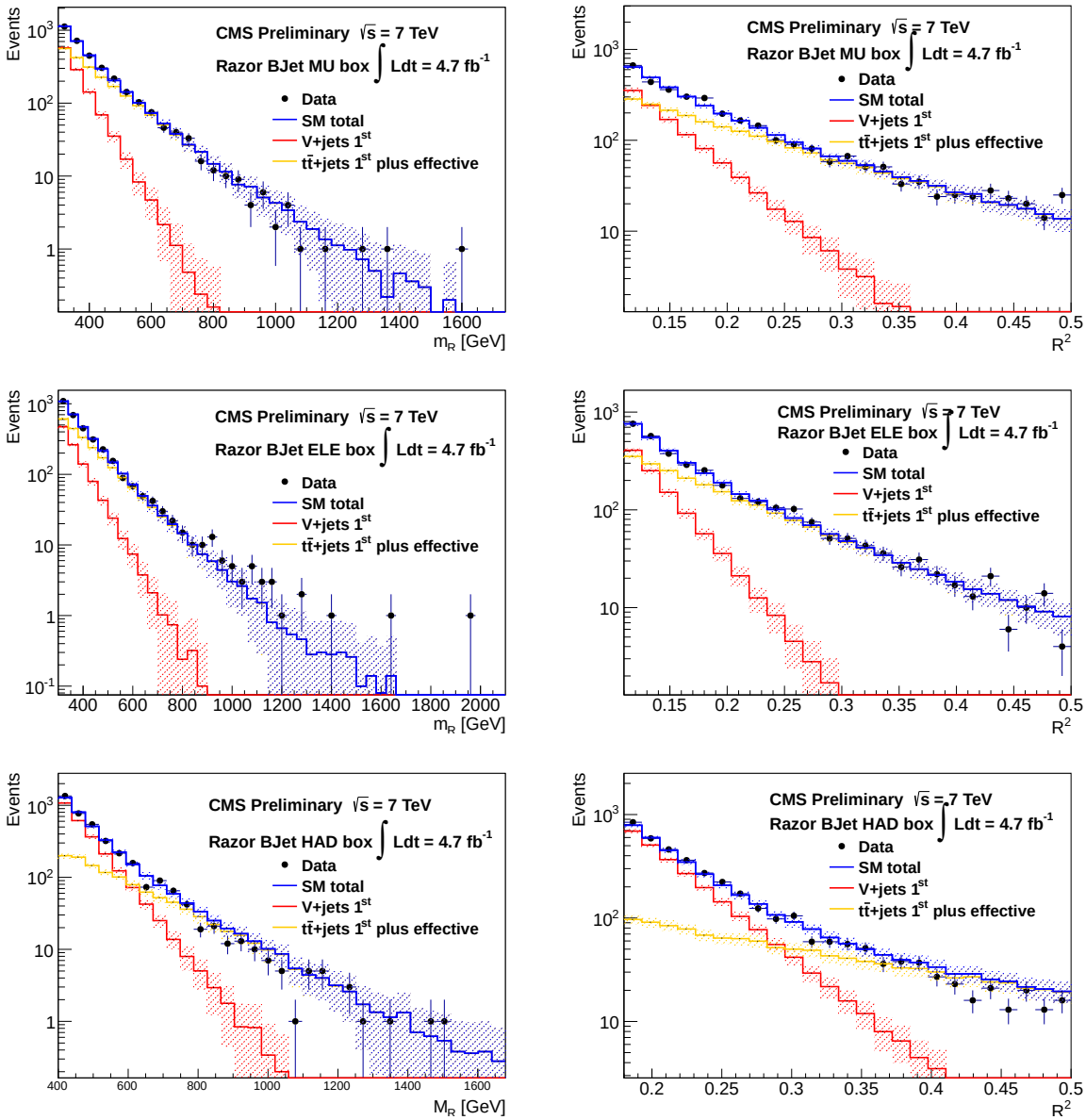

Figure 2: Projection of the 2D fit result on M_R (left) and R^2 (right) for the MU (top), ELE (center), HAD (bottom) b-tagged boxes in the 2011 razor triggered dataset. The blue histogram is the total Standard Model prediction as obtained from a single pseudo-experiment based on the 2D fit. The green, red, and yellow histograms show the breakdown of the Standard Model prediction into separate components as returned by the fit; as verified in simulation, these correspond approximately to the contributions from W,Z + jets and $t\bar{t}$. The fit is performed in the R^2-M_R sideband and projected into the full region. Only the statistical error on the total SM background prediction is shown.

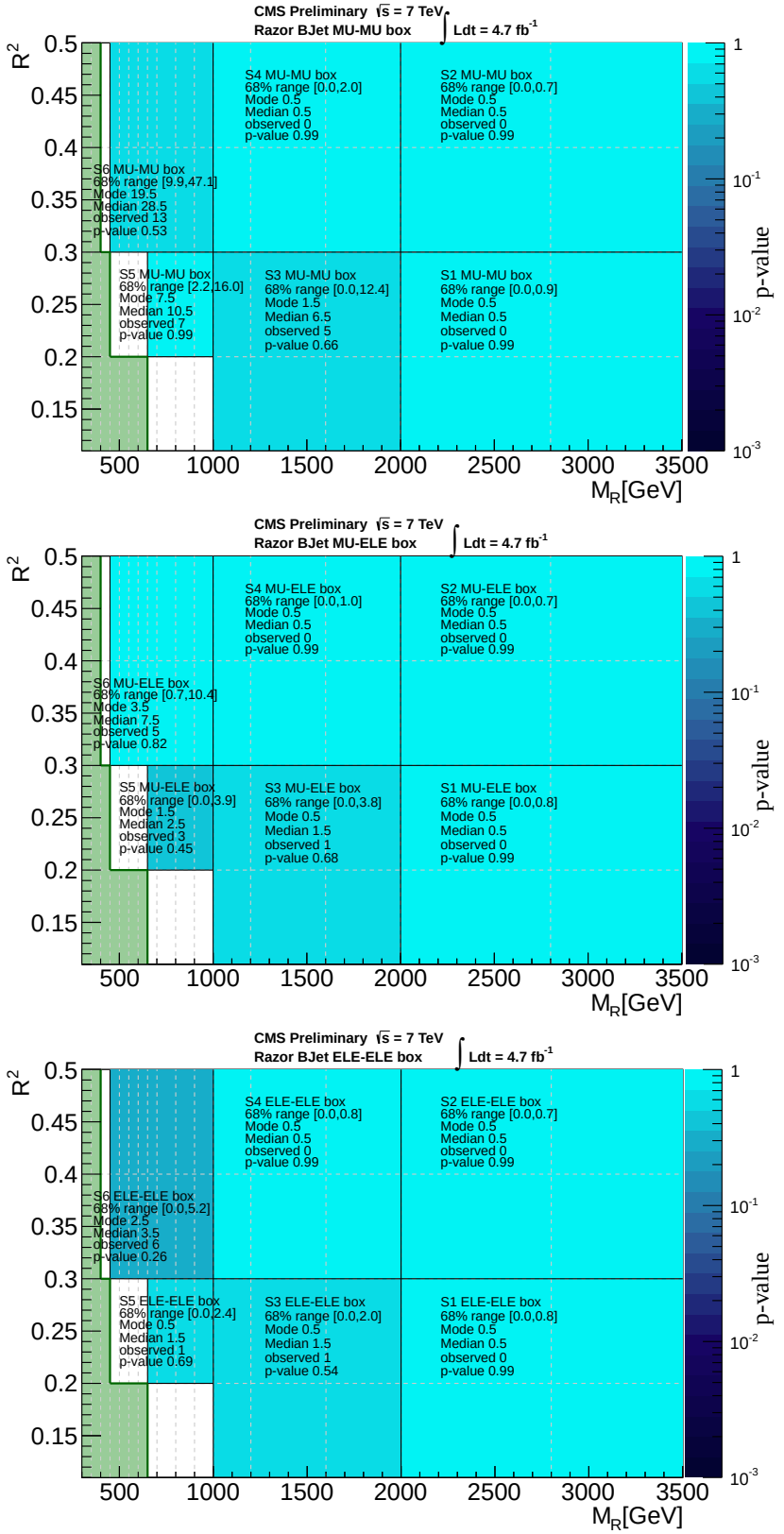

Figure 3: The p-values corresponding to the observed number of events in the MU-MU (top), MU-ELE (center), and ELE-ELE (bottom) b-tagged boxes signal regions defined for this analysis. The green dotted lines indicate the fit regions. The p-values test the compatibility of the observed number of events in data with the SM expectation (obtained from the background parameterization).

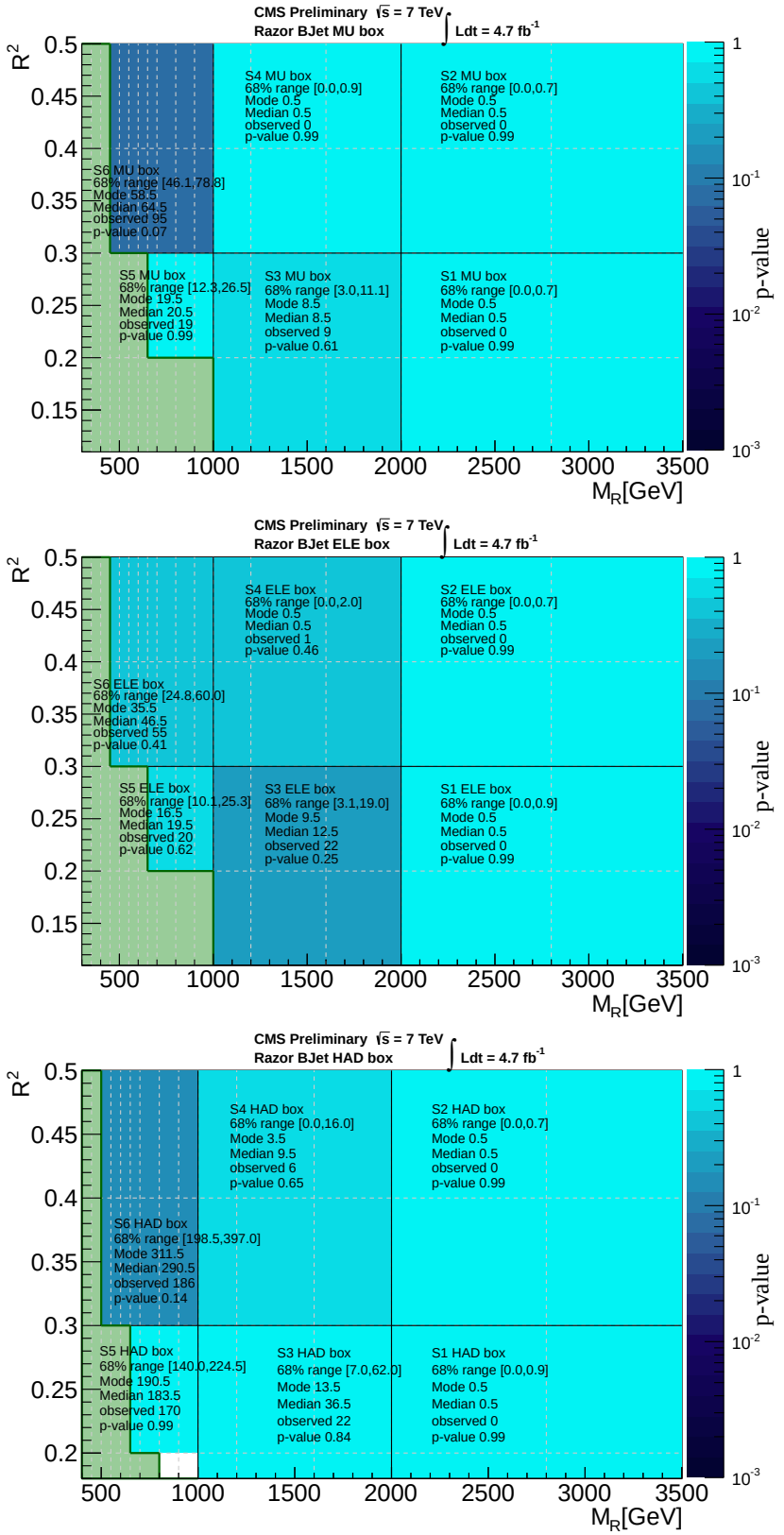

Figure 4: The p-values corresponding to the observed number of events in the MU (top), ELE (middle), and HAD (bottom) b-tagged boxes signal regions defined for this analysis. The green dotted lines indicate the fit regions. The p-values test the compatibility of the observed number of events in data with the SM expectation (obtained from the background parameterization).

background-only likelihood is defined as

$$\mathcal{L}_b = \frac{e^{-(\sum_{SM} N_{SM})}}{N!} \prod_{i=1}^{N} (\sum_{SM} N_{SM} P_{SM}(M_R, R^2)) \,, \tag{7}$$

the same as the fit likelihood except for the fact that we remove the events in the fit region, used to determine the background shape. The signal+background likelihood is written as:

$$\mathcal{L}_{s+b} = \frac{e^{-(\sum_{SM} N_{SM})}}{N!} \prod_{i=1}^{N} (\sum_{SM} N_{SM} P_{SM}(M_R, R^2) + N_S P_S(M_R, R^2)) \tag{8}$$

where N_S is the number of signal events expected for that model at the given luminosity and $P_S(M_R, R^2)$ is the associated pdf.

The signal pdf is described numerically, using a binned 2D histogram made of the signal Monte Carlo events. In order to avoid limited statistics effects in the signal MC samples, we use a variable binning on the 2D plane. On M_R, we use 50 GeV-wide bins starting from the minimal M_R for that box, up to 700 GeV. We then consider the following bin edges:

$$[700, 800, 900, 1000, 1200, 1600, 2000, 2800, 3500] \,. \tag{9}$$

For R^2 we consider the following binning:

$$[R^2_{min}, 0.2, 0.3, 0.4, 0.5] \tag{10}$$

where R^2_{min} is the minimum value of R^2 in the box (0.11 for the leptonic boxes, 0.18 for the hadronic box).

The computation of the CLs proceeds as follows:

- We start from the default signal pdf and a set of alternative pdfs, derived by changing the bin content by the systematic error to that fit. The list of the considered systematic effects is given below. We use log-normal distributions to sample the bin-to-bin shifts for a given toy experiment. Whenever the error is correlated across the R^2 vs. M_R plane, the shift is common across the bins. Otherwise each bin is shifted by an independent amount.
- For each toy experiment, a specific background model is sampled out of the covariance matrix returned by the fit (interpreted as a multi-dimensional Gaussian). This procedure allows to take into account the correlation among the different parameters.
- A sample of events is generated according to these pdfs, both for the signal+background and background-only hypotheses, and the quantity $ln(\mathcal{L}_{s+b}/\mathcal{L}_b)$ is computed.
- The distribution of $ln(\mathcal{L}_{s+b}/\mathcal{L}_b)$ for the signal+background and background-only hypotheses are used to compute the CLs associated to the input cross section for that model.

8.1 Systematic Effects

The error on the knowledge of the background shape is taken into account in the CLs calculation, since the background model changes toy-by-toy according to the covariance matrix returned by the fit.

The list of the systematic effects associated to the signal is given in Tag. 1. The entries labeled as shape systematics correspond to the uncorrelated systematic effect. The size of the effect

depends on the bin in the R^2 versus M_R plane as well as on the model. All the other errors are correlated across the R^2 versus M_R plane. The entries labeled as *point-by-point* also depends on the model under consideration, while the others (e.g. the luminosity error) are constant. Correlation across different boxes is taken into account since the limit-setting procedure runs simultaneously over the six boxes. The systematic error due to the btag efficiency is obtained through the bin-dependent scale factor while the scaling factor is applied to the SUSY MC to correct the efficiency central value by the data-MC difference.

Table 1: Summary of the systematic uncertainties on the signal yield and shape.

yield systematics	
$\mathcal{L}$	2.5%
trigger efficiency R^2-M_R	2%
trigger efficiency lepton	3% (lepton, dilepton boxes)
Btag	$6\% - 20\%$ in p_T bins
shape systematics	
PDF	point-by-point (up to 30%)
JES	point-by-point (up to 1%)
lepton-id (tag-and-probe)	1% (per lepton)

8.2 Simplified Models

We study the analysis sensitivity to a SUSY signal with several SMS benchmark models:

- gluino-gluino production producing 4 b-jets + jets +MET events (T1bbbb) (represented in the top-left image of Fig. 5).
- squark-squark production producing 2 b-jets + jets + MET events (T2bb) (represented in the top-right image of Fig. 5).
- gluino-gluino production producing 4 top + jets +MET events (T1tttt) (represented in the bottom-left image of Fig. 5).
- squark-squark production producing 2 top + jets + MET events (T2tt) (represented in the bottom-right image of Fig. 5).

For each model we show in Fig. 6 the excluded cross section at 95% CL as a function of the mass of the produced particle (gluinos or squarks, depending on the model) and the LSP mass, as well as the exclusion curve corresponding to the NLO+NLL SUSY cross section [26]. We also show exclusion curves for a factor-three cross-section enhancement and decrease.

9 Summary

We performed a search for squarks and gluinos in final states with at least one b-tagged jet using a data sample of $\sim$4.7 fb^{-1} integrated luminosity from pp collisions at $\sqrt{s} = 7$ TeV, recorded by the CMS detector at the LHC. The kinematic consistency of the selected events was tested against the hypothesis of heavy particle pair production using the dimensionless razor variable R related to the missing transverse energy $E_{\mathrm{T}}^{\mathrm{miss}}$, and M_R, an event-by-event indicator of the heavy particle mass scale. In a control dataset we find a simple functional form that describes the distributions of the relevant SM backgrounds as a function of R^2 and M_R. This functional form is used to perform a 2D fit of the SM backgrounds, based on which we predict the background yields and shapes in regions at high mass scale that could contain events from new physics.

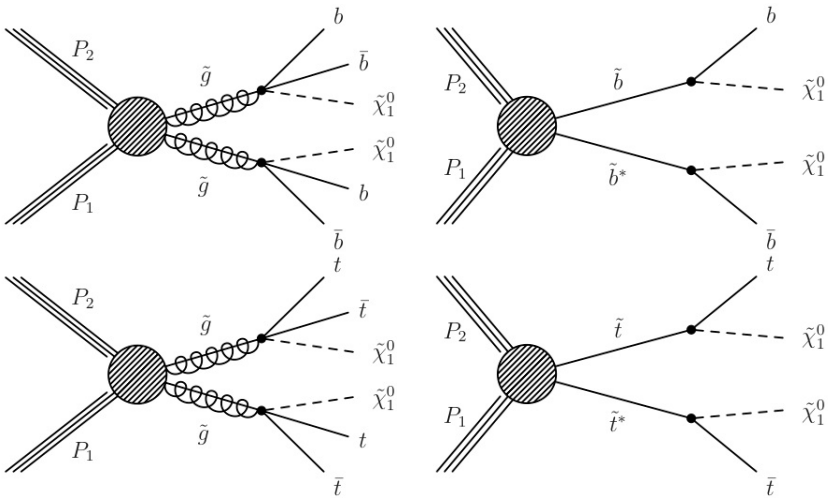

Figure 5: Decay chain associated to the T1bbbb (top-left) and T2bb (top-right), T1tttt (bottom-left) and T2tt (bottom-right) simplified models.

No significant excess over the background expectations was observed and the results were presented as a 95% CL for two b-enriched simplified models.

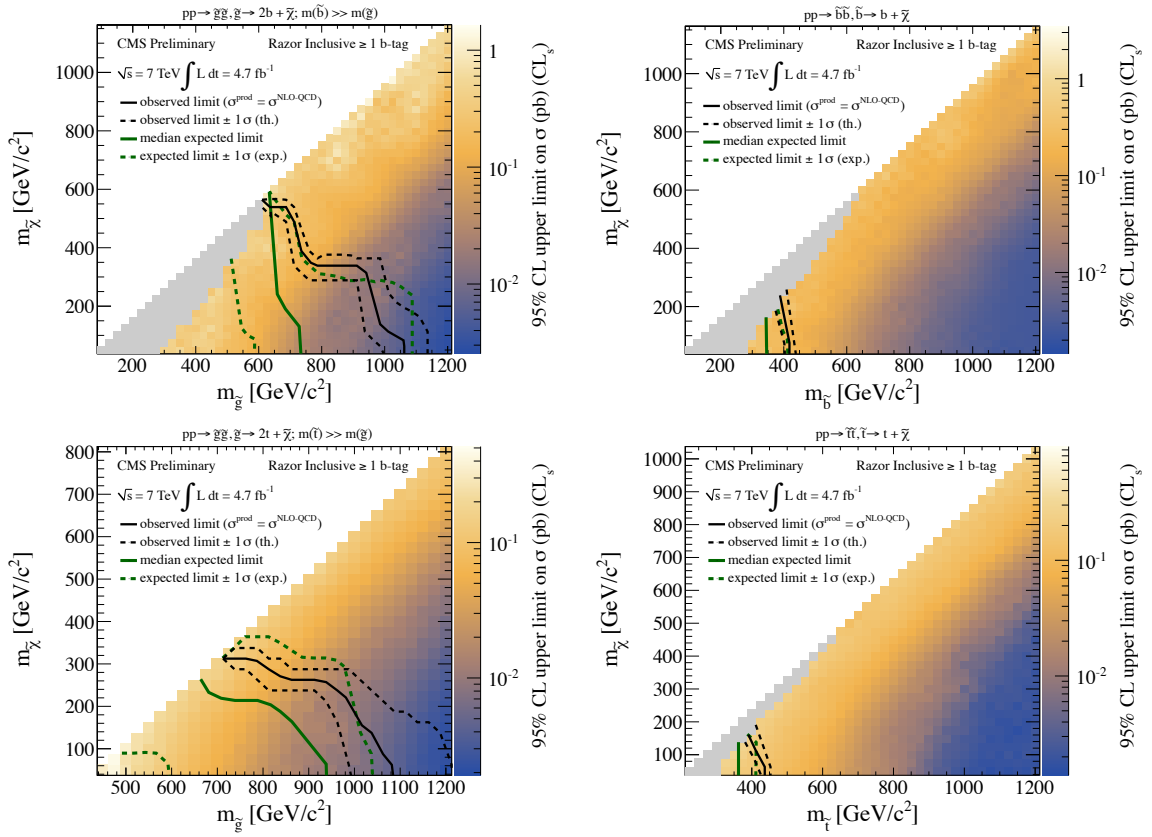

Figure 6: Exclusion cross-section vs. model spectrum for T1bbbb (top-left) and T2bb (top-right), T1tttt (bottom-left) and T2tt (bottom-right).Color-scale (z-axis) indicates the observed cross-section upper limit for each model point, as a function of the mass of the produced particle and the LSP mass. Solid black line indicates observed exclusion region, assuming nominal NLO+NLL SUSY production cross section. Dotted black lines show observed exclusion taking $\pm 1\sigma$ theory errors around nominal cross section. Solid green line indicates median expected exclusion region, with dotted green lines indicating the expected exclusion with $\pm 1\sigma$ experimental uncertainties. The solid grey region indicates model points where the analysis was found to have dependence on ISR modeling in simulation of signal events above a pre-defined tolerance; no interpretation is presented for these model points.

References

[1] C. Rogan, "Kinematics for new dynamics at the LHC", arXiv:1006.2727. CALT-68-2790.

[2] CMS Collaboration, "Inclusive search for squarks and gluinos in pp collisions at sqrt(s) = 7 TeV", arXiv:1107.1279.

[3] CMS Collaboration, "Inclusive search for SUSY using the razor variable in pp Collisions at $\sqrt{s} = 7$ TeV with 0.8/fb", (2011).

[4] CMS Collaboration, "Inclusive search for SUSY using the razor variable in pp Collisions at $\sqrt{s} = 7$ TeV with 4.4/fb", (2012).

[5] CMS Collaboration, "The CMS experiment at the CERN LHC", *JINST* **3** (2008) S08004, doi:10.1088/1748-0221/3/08/S08004.

[6] T. Sjöstrand, S. Mrenna, and P. Skands, "PYTHIA 6.4 Physics and Manual; v6.420, tune D6T", *JHEP* **05** (2006) 026, arXiv:hep-ph/0603175.

[7] F. Maltoni and T. Stelzer, "MadEvent: Automatic event generation with MadGraph", *JHEP* **02** (2003) 027, arXiv:hep-ph/0208156.

[8] GEANT4 Collaboration, "GEANT4: A simulation toolkit", *Nucl. Instrum. Meth.* **A506** (2003) 250–303, doi:10.1016/S0168-9002(03)01368-8.

[9] B. C. Allanach, "SOFTSUSY: a program for calculating supersymmetric spectra", *Comput. Phys. Commun.* **143** (2002) 305–331, doi:10.1016/S0010-4655(01)00460-X, arXiv:hep-ph/0104145.

[10] A. Djouadi, M. M. Muhlleitner, and M. Spira, "Decays of Supersymmetric Particles: the program SUSY-HIT (SUspect-SdecaY-Hdecay-InTerface)", *Acta Phys. Polon.* **B38** (2007) 635–644, arXiv:hep-ph/0609292.

[11] P. Z. Skands et al., "SUSY Les Houches Accord: Interfacing SUSY Spectrum Calculators, Decay Packages, and Event Generators", *JHEP* **07** (2004) 036, doi:10.1088/1126-6708/2004/07/036, arXiv:hep-ph/0311123.

[12] W. Beenakker, R. Hopker, and M. Spira, "PROSPINO: A program for the PROduction of Supersymmetric Particles In Next-to-leading Order QCD", arXiv:hep-ph/9611232.

[13] CMS Collaboration, "Tracking and Primary Vertex Results in First 7 TeV Collisions", *CMS PAS* **TRK-10-005** (2010).

[14] M. Cacciari, G. P. Salam, and G. Soyez, "The anti-kt jet clustering algorithm", *JHEP* **0804** (2008) 063–074, doi:10.1088/1126-6708/2008/04/063.

[15] CMS Collaboration, "Determination of the Jet Energy Scale in CMS with pp Collisions at sqrt(s) = 7 TeV", *CMS PAS* **JME-10-010** (2010).

[16] CMS Collaboration, "Commissioning of the Particle-Flow Reconstruction in Minimum-Bias and Jet Events from pp Collisions at 7 TeV", *CMS PAS* **PFT-10-002** (2010).

[17] CMS Collaboration, "Measurements of Inclusive W and Z Cross Sections in pp Collisions at 7 TeV", *CMS PAS* **EWK-10-002** (2010).

[18] CMS Collaboration, "Commissioning of b-jet identification with pp collisions at sqrt(s) = 7 TeV", *CMS Physics Analysis Summary* **CMS-PAS-BTV-10-001** (2010).

[19] W. Verkerke and D. P. Kirkby, "The RooFit toolkit for data modeling", arXiv:physics/0306116.

[20] R. J. Barlow, "Extended maximum likelihood", *Nucl.Instrum.Meth.* **A297** (1990) 496–506, doi:10.1016/0168-9002(90)91334-8.

[21] B. Knuteson and S. Mrenna, "BARD: Interpreting new frontier energy collider physics", arXiv:hep-ph/0602101.

[22] N. Arkani-Hamed et al., "MARMOSET: The Path from LHC Data to the New Standard Model via On-Shell Effective Theories", arXiv:hep-ph/0703088.

[23] J. Alwall, P. Schuster, and N. Toro, "Simplified Models for a First Characterization of New Physics at the LHC", *Phys. Rev.* **D79** (2009) 075020, doi:10.1103/PhysRevD.79.075020, arXiv:0810.3921.

[24] J. Alwall, M.-P. Le, M. Lisanti et al., "Model-Independent Jets plus Missing Energy Searches", *Phys.Rev.* **D79** (2009) 015005, doi:10.1103/PhysRevD.79.015005, arXiv:0809.3264.

[25] D. Alves et al., "Simplified Models for LHC New Physics Searches", arXiv:1105.2838.

[26] M. Kramer, A. Kulesza, R. van der Leeuw et al., "Supersymmetry production cross sections in pp collisions at sqrts = 7 TeV", arXiv:1206.2892.